



ELSEVIER

Available online at www.sciencedirect.com

SCIENCE @ DIRECT®

Computer Vision
and Image
Understanding

Computer Vision and Image Understanding 98 (2005) 124–154

www.elsevier.com/locate/cviu

Robust real-time eye detection and tracking under variable lighting conditions and various face orientations

Zhiwei Zhu^{a,*}, Qiang Ji^b

^a *Department of Electrical, Computer, and Systems Engineering, Rensselaer Polytechnic Institute
JEC 6219, Troy, NY 12180-3590, USA*

^b *Department of Electrical, Computer, and Systems Engineering, Rensselaer Polytechnic Institute JEC
6044, Troy, NY 12180-3590, USA*

Received 27 July 2004; accepted 27 July 2004

Available online 5 October 2004

Abstract

Most eye trackers based on active IR illumination require distinctive bright pupil effect to work well. However, due to a variety of factors such as eye closure, eye occlusion, and external illumination interference, pupils are not bright enough for these methods to work well. This tends to significantly limit their scope of application. In this paper, we present an integrated eye tracker to overcome these limitations. By combining the latest technologies in appearance-based object recognition and tracking with active IR illumination, our eye tracker can robustly track eyes under variable and realistic lighting conditions and under various face orientations. In addition, our integrated eye tracker is able to handle occlusion, glasses, and to simultaneously track multiple people with different distances and poses to the camera. Results from an extensive experiment shows a significant improvement of our technique over existing eye tracking techniques.

© 2004 Elsevier Inc. All rights reserved.

Keywords: Eye tracking; Support vector machine; Mean shift; Kalman filtering

* Corresponding author.

E-mail addresses: zhuz@rpi.edu (Z. Zhu), qji@ecse.rpi.edu (Q. Ji).

1. Introduction

As one of the salient features of the human face, human eyes play an important role in face detection, face recognition, and facial expression analysis. Robust non-intrusive eye detection and tracking is a crucial step for vision based man-machine interaction technology to be widely accepted in common environments such as homes and offices. Eye tracking has also found applications in other areas including monitoring human vigilance [1], gaze-contingent smart graphics [2], and assisting people with disability. The existing work in eye detection and tracking can be classified into two categories: traditional image-based passive approaches and the active IR based approaches. The former approaches detect eyes based on the unique intensity distribution or shape of the eyes. The underlying assumption is that the eyes appear different from the rest of the face both in shape and intensity. Eyes can be detected and tracked based on exploiting these differences. The active IR based approach, on the other hand, exploits the spectral (reflective) properties of pupils under near IR illumination to produce the bright/dark pupil effect. Eye detection and tracking is accomplished by detecting and tracking pupils.

The traditional methods can be broadly classified into three categories: template based methods [3–9,8,10,11], appearance based methods [12–14] and feature based methods [15–23]. In the template based methods, a generic eye model, based on the eye shape, is designed first. Template matching is then used to search the image for the eyes. Nixon [10] proposed an approach for accurate measurement of eye spacing using Hough transform. The eye is modeled by a circle for the iris and a “tailored” ellipse for the sclera boundary. Their method, however, is time-consuming, needs a high contrast eye image, and only works with frontal faces. Deformable templates are commonly used [3–5]. First, an eye model, which is allowed to translate, rotate and deform to fit the best representation of the eye shape in the image, is designed. Then, the eye position can be obtained through a recursive process in an energy minimization sense. While this method can detect eyes accurately, it requires the eye model be properly initialized near the eyes. Furthermore, it is computationally expensive, and requires good image contrast for the method to converge correctly.

The appearance based methods [12–14] detect eyes based on their photometric appearance. These methods usually need to collect a large amount of training data, representing the eyes of different subjects, under different face orientations, and under different illumination conditions. These data are used to train a classifier such as a neural network or the support vector machine and detection is achieved via classification. Pentland et al. [12] extended the eigenface technique to the description and coding of facial features, yielding eigeneyes, eigen noses, and eigenmouths. For eye detection, they extracted an appropriate eye templates for training and constructed a principal component projective space called “Eigeneyes.” Eye detection is accomplished by comparing a query image with an eye image in the eigeneyes space. Huang et al. [13] also employed the eigeneyes to perform initial eye positions detection. Huang et al. [14] presented a method to represent eye image using wavelets and to perform eye detection using RBF NN classifier. Reinders et al. [21] proposed several improvements on the neural network based eye detector. The trained neural

network eye detector can detect rotated or scaled eyes under different lighting conditions. But it is trained for the frontal view face image only.

Feature based methods explore the characteristics (such as edge and intensity of iris, the color distributions of the sclera and the flesh) of the eyes to identify some distinctive features around the eyes. Kawato et al [16] proposed a feature based method for eyes detection and tracking. Instead of detecting eyes, they proposed to detect the point between two eyes. The authors believe the point is more stable and easier to detect than the eyes. Eyes are subsequently detected as two dark parts, symmetrically located on each side of the between-eye-point. Feng et al. [8,9] designed a new eye model consisting of six landmarks (eye corner points). Their technique first locates the eye landmarks based on the variance projection function (VPF) and the located landmarks are then employed to guide the eye detection. Experiment shows their method will fail if the eye is closed or partially occluded by hair or face orientation. In addition, their technique may mistake eyebrows for eyes. Tian et al. [19] proposed a new method to track the eye and recover the eye parameters. The method requires to manually initialize the eye model in the first frame. The eye's inner corner and eyelids are tracked using a modified version of the Lucas–Kanade tracking algorithm [24]. The edge and intensity of iris are used to extract the shape information of the eye. Their method, however, requires a high contrast image to detect and track eye corners and to obtain a good edge image.

In summary, the traditional image based eye tracking approaches detect and track the eyes by exploiting eyes' differences in appearance and shape from the rest of the face. The special characteristics of the eye such as dark pupil, white sclera, circular iris, eye corners, eye shape, etc. are utilized to distinguish the human eye from other objects. But due to eye closure, eye occlusion, variability in scale and location, different lighting conditions, and face orientations, these differences will often diminish or even disappear. Wavelet filtering [25,26] has been commonly used in computer vision to reduce illumination effect by removing subbands sensitive to illumination change. But it only works under slight illumination variation. Illumination variation for eye tracking applications could be significant. Hence, the eye image will not look much different in appearance or shape from the rest of the face, and the traditional image based approaches can not work very well, especially for faces with non-frontal orientations, under different illuminations, and for different subjects.

Eye detection and tracking based on the active remote IR illumination is a simple yet effective approach. It exploits the spectral (reflective) properties of the pupil under near IR illumination. Numerous techniques [27–31,1] have been developed based on this principle, including some commercial eye trackers [32,33]. They all rely on an active IR light source to produce the dark or bright pupil effects. Ebisawa et al. [27] generate the bright/dark pupil images based on a differential lighting scheme using two IR light sources (on and off camera axis). The eye can be tracked effectively by tracking the bright pupils in the difference image resulting from subtracting the dark pupil image from the bright pupil image. Later in [28], they further improved their method by using pupil brightness stabilization to eliminate the glass reflection. Morimoto et al. [29] also utilize the differential lighting scheme to generate the bright/dark pupil images, and pupil detection is done after thresholding the

difference image. A larger temporal support is used to reduce artifacts caused mostly by head motion, and geometric constraints are used to group the pupils.

Most of these methods require distinctive bright/dark pupil effect to work well. The success of such a system strongly depends on the brightness and size of the pupils, which are often affected by several factors including eye closure, eye occlusion due to face rotation, external illumination interferences, and the distances of the subjects to the camera. Figs. 1 and 2 summarize different conditions under which the pupils may not appear very bright or even disappear. These conditions include eye closure (Fig. 1A) and oblique face orientations (Figs. 1B–D), presence of other bright objects (due to either eye glasses glares or motion) as shown in Figs. 2A and B, and external illumination interference as shown in Fig. 2C.

The absence of the bright pupils or even weak pupil intensity poses serious problems to the existing eye tracking methods using IR for they all require relatively stable lighting conditions, users close to the camera, small out-of-plane face rotations, and open and un-occluded eyes. These conditions impose serious restrictions on the part of their systems as well as on the user, and therefore limit their application scope. Realistically, however, lighting can be variable in many application domains,

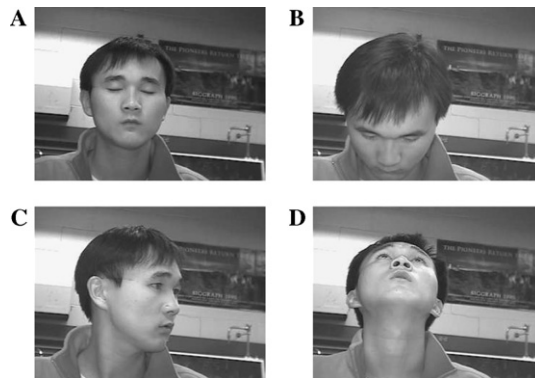


Fig. 1. The disappearance of the bright pupils due to eye closure (A) and oblique face orientations (B), (C), and (D).

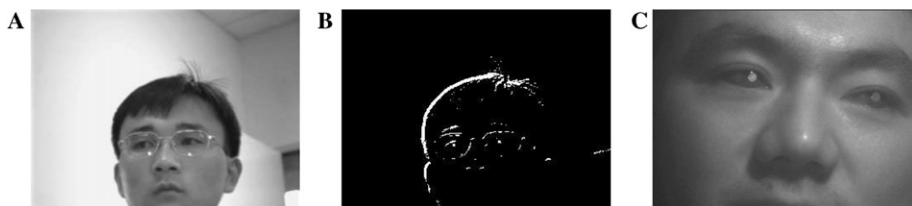


Fig. 2. (A) Original image, (B) the corresponding thresholded difference image, which contains other bright regions around the real pupil blobs due to either eye glasses glares and rapid head motion, (C) Weak pupils intensity due to strong external illumination interference.

the natural movement of head often involves out-of-plane rotation, eye closures due to blinking, and winking are physiological necessities for humans. Furthermore, thick eye glasses tend to disturb the infrared light so much that the pupils appear very weak. It is therefore very important for the eye tracking system to be able to robustly and accurately track eyes under these conditions as well.

To alleviate some of these problems, Ebisawa [28] proposed an image difference method based on two light sources to perform pupil detection under various lighting conditions. The background can be eliminated using the image difference method and the pupils can be easily detected by setting the threshold as low as possible in the difference image. They also proposed an ad hoc algorithm for eliminating the glares on the glasses, based on thresholding and morphological operations. However, the automatic determination of the threshold and the structure element size for morphological operations is difficult; and the threshold value cannot be set as low as possible considering the efficiency of the algorithm. Also, eliminating the noise blobs just according to their sizes is not enough. Haro [31] proposed to perform pupil tracking based on combining eye appearance, the bright pupil effect, and motion characteristics so that pupils can be separated from other equally bright objects in the scene. To do so, they proposed to verify the pupil blobs using conventional appearance based matching method and the motion characteristics of the eyes. But their method cannot track the closed or occluded eyes or eyes with weak pupil intensity due to external illuminations interference. Ji et al. [1] proposed a real time subtraction and a special filter to eliminate the external light interferences. But their technique fails to track the closed/occluded eyes. To handle the presence of other bright objects, their method performs pupil verification based on the shape and size of pupil blobs to eliminate spurious pupils blobs. But usually, spurious blobs have similar shape and size to those of the pupil blobs as shown in Fig. 2 and make it difficult to distinguish the real pupil blobs from the noise blobs based on only shape and size.

In this paper, we propose a real-time robust method for eye tracking under variable lighting conditions and face orientations, based on combining the appearance-based methods and the active IR illumination approach. Combining the respective strengths of different complementary techniques and overcoming their shortcomings, the proposed method uses an active infrared illumination to brighten subject's faces to produce the bright pupil effect. The bright pupil effect and the appearance of eyes are utilized simultaneously for eyes detection and tracking. The latest technologies in pattern classification recognition (the support vector machine) and in object tracking (the mean-shift) are employed for pupil detection and tracking based on eyes appearance. Some of the ideas presented in this paper have been briefly reported in [34,35]. In this paper, we report our algorithm in details.

Our method consists of two parts: eye detection and eye tracking. Eye detection is accomplished by simultaneously utilizing the bright/dark pupil effect under active IR illumination and the eye appearance pattern under ambient illumination via the support vector machine. Eye tracking is composed of two major modules. The first module is a conventional Kalman filtering tracker based on the bright pupil. The Kalman filtering tracker is augmented with the support vector machine classifier [36,37] to

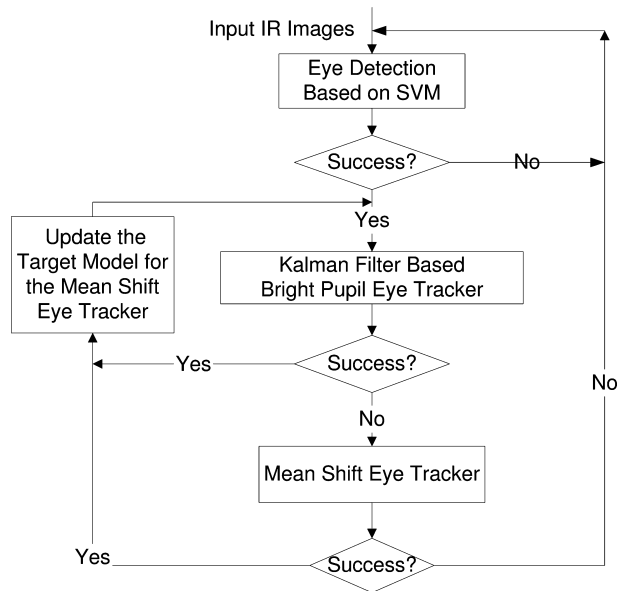


Fig. 3. The combined eye tracking flowchart.

perform verification of the detected eyes. In case Kalman eye tracker fails due to either weak pupil intensity or the absence of the bright pupils, eye tracking based on mean shift is activated [38] to continue tracking the eyes. Eye tracking returns to the Kalman filtering tracker as soon as the bright pupils reappear since eye tracking using bright pupils is much more robust than the mean shift tracker, which, we find, tends to drift away. The two trackers alternate, complementing each other and overcoming their limitations. Fig. 3 summarizes our eye tracking algorithm.

2. Eye detection

To facilitate subsequent image processing, the person's face is illuminated using a near-infrared illuminator. The use of infrared illuminator serves three purposes: first it minimizes the impact of different ambient light conditions, therefore ensuring image quality under varying real-world conditions including poor illumination, day, and night; second, it allows to produce the bright/dark pupil effect, which constitutes the foundation for the proposed eye detection and tracking algorithm. Third, since near infrared is barely visible to the user, this will minimize any interference with the user's work. According to the original patent from Hutchinson [39], a bright pupil can be obtained if the eyes are illuminated with a near infrared illuminator beaming light along the camera optical axis at certain wavelength. At the near infrared wavelength, pupils reflect almost all infrared light they receive along the path back to the camera, producing the bright pupil effect, very much similar to the red eye effect in

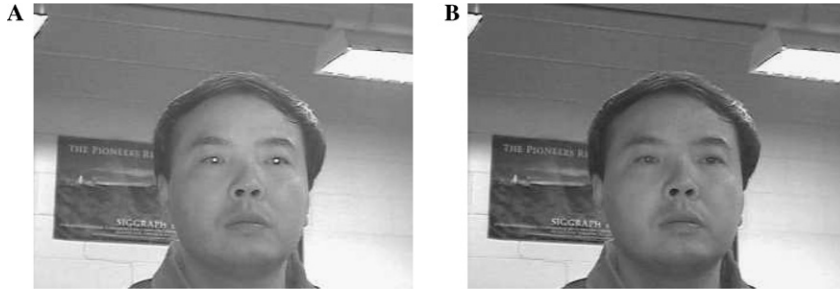


Fig. 4. The bright (A) and dark (B) pupils images.

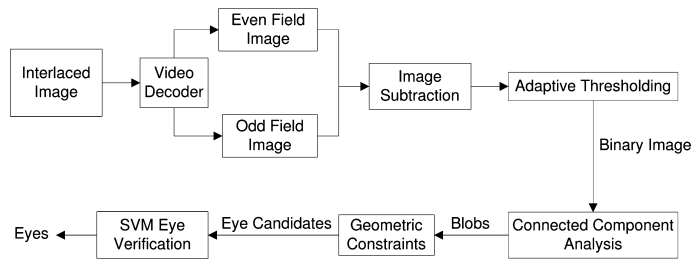


Fig. 5. Eye detection block diagram.

photography. If illuminated off the camera optical axis, the pupils appear dark since the reflected light will not enter the camera lens. This produces the so called dark pupil effects. An example of the bright/dark pupils is given in Fig. 4. Details about the construction of the IR illuminator and its configuration may be found in [40].

Given the IR illuminated eye images, eye detection is accomplished via pupil detection. Pupil detection is accomplished based on both the intensity of the pupils (the bright and dark pupils) and on the appearance of the eyes using the support vector machine. Specifically, pupil detection starts with preprocessing to remove external illumination interference, followed by searching the whole image for pupils in terms of pupil intensity and eye appearance. Therefore, multiple pupils can be detected if there exist more than one person. The use of support vector machine (SVM) avoids falsely identifying a bright region as a pupil. Fig. 5 gives an overview of the eye detection module.

2.1. Initial eye position detection

The detection algorithm starts with a preprocessing to minimize interference from illumination sources other than the IR illuminator. This includes sunlight and ambient light interference. A differential method is used to remove the background interference by subtracting the dark eye image (odd field) from the bright eye image (even field), producing a difference image, with most of the background and external illu-

mination effects removed, as shown in Fig. 6. For real time eye tracking, the image subtraction must be implemented efficiently in real time. To achieve this, we developed circuitry to synchronize the outer ring of LEDs and inner ring of LEDs with the even and odd fields of the interlaced image, respectively, so that they can be turned on and off alternately. When the even field is being scanned, the inner ring of LEDs is on and the outer ring of LEDs is off and vice versa when the even field is scanned. The interlaced input image is subsequently de-interlaced via a video decoder, producing the even and odd field images as shown in Figs. 6A and B. More on our image subtraction circuitry may be found in [40].

The difference image is subsequently thresholded automatically based on its histogram, producing a binary image. Connected component analysis is then applied to the binary image to identify the binary blobs. Our task is then to find out which of the blobs actually is the real pupil blob. Initially, we mark all the blobs as potential candidates for pupils as shown in Fig. 7.

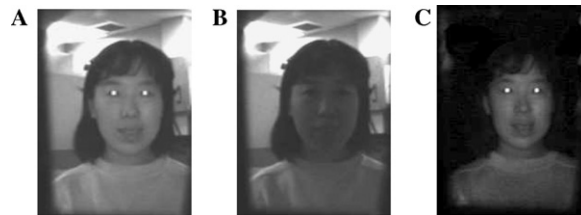


Fig. 6. Background illumination interference removal (A) the even image field obtained with both ambient and IR light; (B) the odd image field obtained with only ambient light; (C) the image resulted from subtraction (B) from (A).

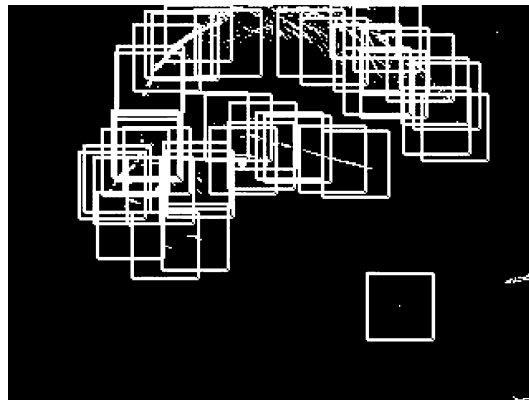


Fig. 7. The thresholded difference image marked with pupil candidates.

2.2. Eye verification using support vector machine

As shown in Fig. 7, there are usually many potential candidates of pupils. Typically, pupils are found among the binary blobs. However, it is usually not possible to isolate the pupil blob only by picking the right threshold value, since pupils are often small and not bright enough compared with other noise blobs. Thus, we will have to make use of information other than intensity to correctly identify them. One initial way to distinguish the pupil blobs from other noise blobs is based on their geometric shapes. Usually, the pupil is an ellipse-like blob and we can use an ellipse fitting method [41] to extract the shape of each blob and use the shape and size to remove some blobs from further consideration. It must be noted, however, that due to scale change (distance to the camera) and to variability in individual pupil size, size is not a reliable criterion. It is only used to remove very large or very small blobs. Shape criterion, on the other hand, is scale-invariant. Nevertheless, shape alone is not sufficient since there are often present other non-pupil blobs with similar shape and size as shown in Fig. 8, where we can see that there are still several non-pupil blobs left because they are so similar in shape and size that we can not distinguish the real pupil blobs from them. So we have to use other features. We observed that the eye region surrounding pupils has a unique intensity distribution. They appear different from other parts of the face in the dark pupil image as shown in Fig. 4B. The appearance of an eye can therefore be utilized to separate it from non-eyes. We map the locations of the remaining binary blobs to the dark pupil images and then apply the support vector machine (SVM) classifier [36,37] to automatically identify the binary blobs that correspond to eyes as discussed below.

2.2.1. The support vector machine

SVM is a two-class classification method that finds the optimal decision hyperplane based on the concept of structural risk minimization. Ever since its introduction, SVM [36] has become increasingly popular. The theory of SVM can be briefly summarized as follows. For the case of two-class pattern recognition, the task of



Fig. 8. The thresholded difference image after removing some blobs based on their geometric properties (shape and size). The blobs marked with circles are selected for further consideration.

predictive learning from examples can be formulated as follows. Given a set of functions f_α and an input domain R^N of N dimensions:

$$\{f_\alpha : \alpha \in A\}, f_\alpha : R^N \rightarrow \{-1, +1\},$$

(A is an index set) and a set of l examples:

$$(x_1, y_1), \dots, (x_i, y_i), \dots, (x_l, y_l), \quad x_i \in R^N, \quad y_i \in \{-1, +1\},$$

where x_i is an input feature vector and y_i represents the class, which has only two values -1 and $+1$. Each (x_i, y_i) is generated from an unknown probability distribution $p(x, y)$, the goal is to find a particular function f_α^* which provides the smallest possible value for the risk:

$$R(\alpha) = \int |f_\alpha(x) - y| dp(x, y). \quad (1)$$

Suppose that there is a separating hyper-plane that separates the positive class from the negative class. The data characterizing the boundary between the two classes are called the support vectors since they alone define the optimal hyper-plane. First, a set (x_i, y_i) of labeled training data are collected as the input to the SVM. Then, a trained SVM will be characterized by a set of N_s support vectors s_i , coefficient weights α_i for the support vectors, class labels y_i of the support vectors, and a constant term w_0 .

For the linearly separable case, the linear decision surface (the hyperplane) is defined as

$$w \cdot x + w_0 = 0, \quad (2)$$

where x is a point the hyperplane, “ \cdot ” denotes dot product, w is the normal of the hyperplane, and w_0 is the distance to the hyperplane from the origin. Through the use of training data, w can be estimated by

$$w = \sum_{i=1}^{N_s} \alpha_i y_i s_i, \quad (3)$$

Given w and w_0 , an input vector x_i can be classified into one of the two classes, depending on if $w \cdot x + w_0$ is larger or smaller than 0.

Classes are often not linearly separable. In this case, SVM can be extended by using a kernel $K(\cdot, \cdot)$, which performs a non-linear mapping of the feature space to a higher dimension, where classes are linearly separable. The most common SVM kernels include Gaussian kernel, Radial-based kernel, and polynomial kernel. The decision rule with a kernel can be expressed as

$$\sum_{i=1}^{N_s} \alpha_i y_i K(s_i, x) + w_0 = 0. \quad (4)$$

2.2.2. SVM training

To use SVM, training data are needed to obtain the optimal hyper-plane. An eye image is represented as a vector I consisting of the original pixel values. For this

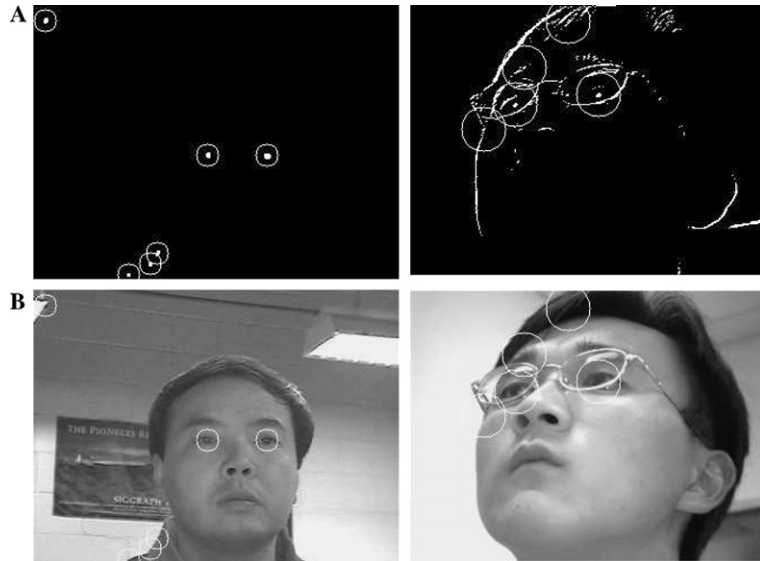


Fig. 9. (A) The thresholded difference image superimposed with possible pupil candidates. (B) The dark image marked with possible eye candidates according to the positions of pupil candidates in (A).

project, after obtaining the positions of pupil candidates using the methods mentioned above, we obtain the sub-images from the dark image according to those positions as shown in Fig. 9.

Usually, the eyes are included in those cropped images of 20×20 pixels. The cropped image data are processed using histogram equalization and normalized to a $[0, 1]$ range before training. The eye training images were divided into two sets: positive set and negative set. In the positive image set, we include eye images of different gazes, different degrees of opening, different face poses, different subjects, and with/without glasses. The non-eye images were placed in the negative image set. Figs. 10 and 11 contain examples of eye and non-eye images in the training sets, respectively.

After finishing the above step, we get a training set, which has 558 positive images and 560 negative images. In order to obtain the best accuracy, we need to identify the best parameters for the SVM. In Table 1, we list three different SVM kernels with various parameter settings and each SVM was tested on 1757 eye candidate images obtained from different persons.

From the above table, we can see that the best accuracy we can achieve is 95.5037%, using a Gaussian kernel with a σ of 3.

2.2.3. Retraining using mis-labeled data

Usually, supervised learning machines rely only on the limited labeled training examples and cannot reach very high learning accuracy. So we have to test on thousands of unlabeled data and pick up the mis-labeled data, then put them into the correct training sets and retrain the classifier again. After performing this procedure on



Fig. 10. The eye images in the positive training set.

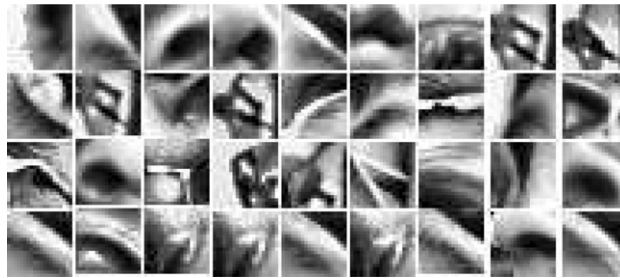


Fig. 11. The non-eye images in the negative training set.

Table 1
Experiment results using 3 kernels with different parameters

Kernel type	Deg	Sigma σ	# Support vectors	Accuracy
Linear			376	0.914058
Polynomial	2		334	0.912351
Polynomial	3		358	0.936255
Polynomial	4		336	0.895845
Gaussian		1	1087	0.500285
Gaussian		2	712	0.936255
Gaussian		3	511	0.955037
Gaussian		4	432	0.9465
Gaussian		5	403	0.941377

the unlabeled data obtained from different conditions several times, we can boost the accuracy of the learning machine at the cost of extra time needed for re-training.

Specifically, we have eye data set from 10 people, which are obtained using the same method. We choose the first person's data set and label the eye images and non-eye images manually, then we train the Gaussian SVM on this training set and test Gaussian SVM on the second person's data set. We check the second person's data one by one, pick up all the mis-labeled data, label them correctly and add them into the training set. After finishing the above step, we retrain the SVM

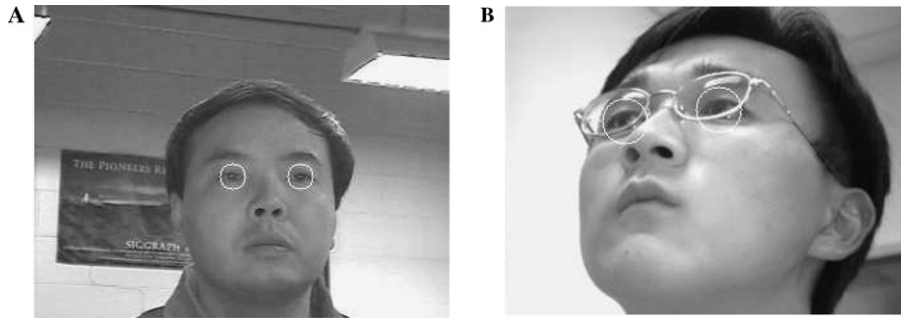


Fig. 12. (A,B) The images marked with identified eyes. Compared with images in Fig. 9B, many false alarms have been removed.

on this increased training set and repeat the above step on the next person's data set. The whole process then repeats until the classification errors stabilize. Through the retraining process, we can significantly boost the accuracy of the Gaussian SVM.

2.2.4. Eye detection with SVM

During eye detection, we crop the regions in the dark pupil image according to the locations of pupil candidates in the difference image as shown in Fig. 9B. After some preprocessing on these eye candidate images, they will be provided to the trained SVM for classification. The trained SVM will classify the input vector I into eye class or non-eye class. Fig. 12 shows that the SVM eye classifier correctly identifies the real eye regions as marked.

Pupil verification with SVM works reasonably well and can generalize to people of the same race. However, for people from a race that is significantly different from those in training images, the SVM may fail and need to be retrained. SVM can work under different illumination conditions due to the intensity normalization for the training images via histogram equalization.

3. Eye tracking algorithm

Given the detected eyes in the initial frames, the eyes in subsequent frames can be tracked from frame to frame. Eye tracking can be done by performing pupil detection in each frame. This brute force method, however, will significantly slow down the speed of pupil tracking, making real time pupil tracking impossible since it needs to search the entire image for each frame. This can be done more efficiently by using the scheme of prediction and detection. Kalman filtering [42] provides a mechanism to accomplish this. The Kalman pupil tracker, however, may fail if pupils are not bright enough under the conditions mentioned previously. In addition, rapid head movement may also cause the tracker to lose the eyes. This problem is addressed by augmenting the Kalman tracker with the mean shift tracker. Fig. 13 summarizes our eye tracking scheme. Specifically, after locating the eyes in the initial frames,

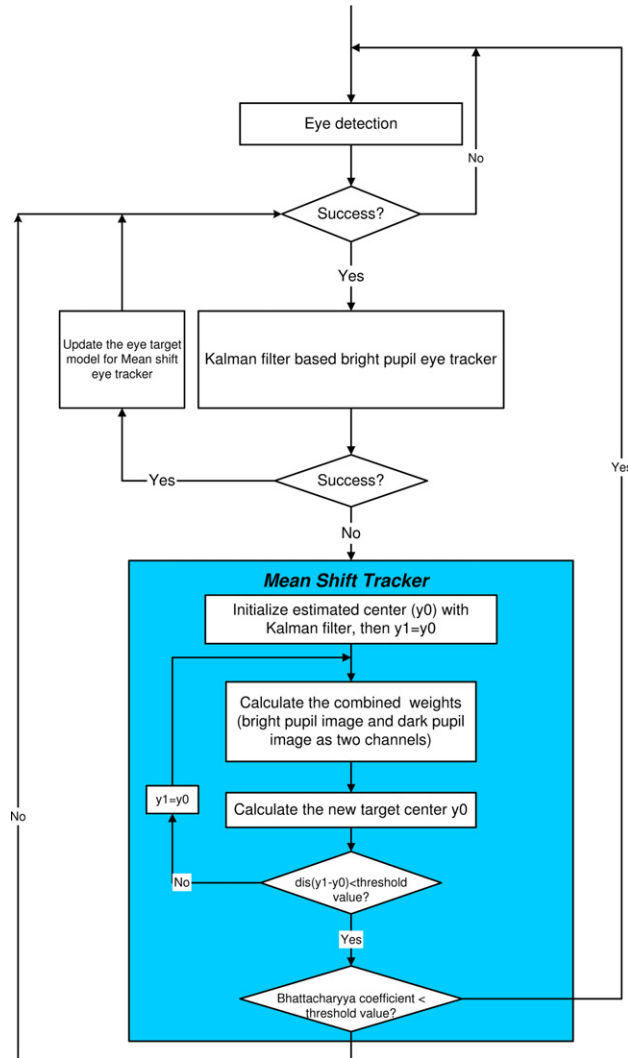


Fig. 13. The combined eye tracking flowchart.

Kalman filtering is activated to track bright pupils. If it fails in a frame due to disappearance of bright pupils, eye tracking based on the mean shift will take over. Our eye tracker will return to bright pupil tracking as soon as bright pupil appears again since it is much more robust and reliable tracking. Pupil detection will be activated if the mean shift tracking fails. These two stage eye trackers work together and they complement each other. The robustness of the eye tracker is improved significantly. The Kalman tracking, the mean shift tracking, and their integration are briefly discussed below.

3.1. Eye (pupil) tracking with kalman filtering

A Kalman filter is a set of recursive algorithms that estimate the position and uncertainty of moving targets in the next time frame, that is, where to look for the targets, and how large a region should be searched in the next frame around the predicted position in order to find the targets with certain confidence. It recursively conditions current estimate on all of the past measurements and the process is repeated with the previous posterior estimates used to project the new a priori estimates. This recursive nature is one of the very appealing features of the Kalman filter since it makes practical implementation much more feasible.

Our pupil tracking method based on Kalman filtering can be formalized as follows. The state of a pupil at each time instance (frame) t can be characterized by its position and velocity. Let (c_t, r_t) represent the pupil pixel position (its centroid) at time t and (u_t, v_t) be its velocity at time t in c and r directions, respectively. The state vector at time t can therefore be represented as $X_t = (c_t \ r_t \ u_t \ v_t)^T$.

According to the theory of Kalman filtering [43], X_{t+1} , the state vector at the next time frame $t+1$, linearly relates to current state X_t by the system model as follows:

$$X_{t+1} = \Phi X_t + W_t, \quad (5)$$

where Φ is the state transition matrix and W_t represents system perturbation. W_t is normally distributed as $p(W_t) \sim N(0, Q)$, and Q represents the process noise covariance.

We further assume that a fast feature extractor estimates $Z_t = (\hat{c}_t, \hat{r}_t)$, the detected pupil position at time t . Therefore, the measurement model in the form needed by the Kalman filter is

$$Z_t = HX_t + M_t, \quad (6)$$

where matrix H relates current state to current measurement and M_t represents measurement uncertainty. M_t is normally distributed as $p(M_t) \sim N(0, R)$, and R is the measurement noise covariance. For simplicity and since Z_t only involves position, H can be represented as

$$H = \begin{bmatrix} 1 & 0 & 0 & 0 \\ 0 & 1 & 0 & 0 \end{bmatrix}.$$

The feature detector (e.g., thresholding or correlation) searches the region as determined by the projected pupil position and its uncertainty to find the feature point at time $t+1$. The detected point is then combined with the prediction estimation to produce the final estimate.

Specifically, given the state model in Eq. (5) and measurement model in Eq. (6) as well as some initial conditions, the state vector X_{t+1} , along with its covariance matrix Σ_{t+1} , can be updated as follows. For subsequent discussion, let us define a few more variables. Let X_{t+1}^- be the estimated state at time $t+1$, resulting from using the system model only. It is often referred to as the prior state estimate. X_{t+1} differs from X_{t+1}^- in that it is estimated using both the system model Eq. (5) and the measurement model Eq. (6). X_{t+1} is usually referred as the posterior state estimate. Let Σ_{t+1}^- and

Σ_{t+1} be the covariance matrices for the state estimates X_{t+1}^- and X_{t+1} , respectively. They characterize the uncertainties associated with the prior and posterior state estimates. The goal of Kalman filtering is therefore to estimate X_{t+1} and Σ_{t+1} given X_t , Σ_t , Z_t , and the system and measurement models. The Kalman filtering algorithm for state prediction and updating may be summarized below.

1. State prediction

Given current state X_t and its covariance matrix Σ_t , state prediction involves two steps: state projection (X_{t+1}^-) and error covariance estimation (Σ_{t+1}^-) as summarized in Eq. (7) and Eq. (8).

$$X_{t+1}^- = \Phi X_t, \quad (7)$$

$$\Sigma_{t+1}^- = \Phi \Sigma_t \Phi^T + Q_t. \quad (8)$$

Given the prior estimate X_{t+1}^- , its covariance matrix Σ_{t+1}^- , pupil detection is performed to detect the pupil around X_{t+1}^- , with the search area determined by Σ_{t+1}^- . In practice, to speed up the computation, the values of $\Sigma_{t+1}^- [0][0]$ and $\Sigma_{t+1}^- [1][1]$ are used to compute the search area size. Specifically, the search area size is chosen as $20 + 2 * \Sigma_{t+1}^- [0][0]$ pixels and $20 + 2 * \Sigma_{t+1}^- [1][1]$ pixels, where 20×20 pixels is the basic window size. This means the larger the $\Sigma_{t+1}^- [0][0]$ and $\Sigma_{t+1}^- [1][1]$ are, the more uncertainty of the estimation is, and the larger the search area is. The search area is therefore adaptively adjusted. Therefore, the pupil can be located quickly.

2. State updating

The detected pupil position is represented by Z_{t+1} . Then, state updating can be performed to derive the final state and its covariance matrix. The first task during state updating is to compute the Kalman gain K_{t+1} . It is done as follows:

$$K_{t+1} = \frac{\Sigma_{t+1}^- H^T}{H \Sigma_{t+1}^- H^T + R}. \quad (9)$$

The gain matrix K can be physically interpreted as a weighting factor to determine the contribution of measurement Z_{t+1} and prediction HX_{t+1}^- to the posterior state estimate X_{t+1} . The next step is to generate a posteriori state estimate X_{t+1} by incorporating the measurement into Eq. (5). X_{t+1} is computed as follows:

$$X_{t+1} = X_{t+1}^- + K_{t+1}(Z_{t+1} - HX_{t+1}^-). \quad (10)$$

The final step is to obtain the posteriori error covariance estimate. It is computed as follows:

$$\Sigma_{t+1} = (I - K_{t+1}H)\Sigma_{t+1}^-. \quad (11)$$

After each time and measurement update pair, the Kalman filter recursively conditions current estimate on all of the past measurements and the process is repeated with the previous posterior estimates used to project a new a priori estimate.

The Kalman filter pupil tracker works reasonably well under frontal face rotation with the eye open. However, it will fail if the pupils are not bright due to either face

orientation or external illumination interferences. The Kalman filter also fails when a sudden head movement occurs due to incorrect prediction because the assumption of smooth head motion has been violated. In each case, Kalman filtering fails because the Kalman filter detector can not detect pupils. We propose to use the mean shift tracking to augment Kalman filtering tracking to overcome this limitation.

3.2. Mean shift eye tracking

Due to the IR illumination, the eye region in the dark and bright pupil images exhibits strong and unique visual patterns such as the dark iris in the white part. This unique pattern should be utilized to track eyes in case the bright pupils fail to appear on the difference images. This is accomplished via the use of the mean shift tracking. Mean shift tracking is an appearance based object tracking method. It employs mean shift analysis to identify a target candidate region, which has the most similar appearance to the target model in terms of intensity distribution.

3.2.1. Similarity measure

The similarity of two distributions can be expressed by a metric based on the Bhattacharyya coefficient as described in [38]. The derivation of the Bhattacharyya coefficient from sample data involves the estimation of the target density q and the candidate density p , for which we employ the histogram formulation. Therefore, the discrete density $\hat{q} = \{\hat{q}_u\}_{u=1..m}$ (with $\sum_{u=1}^m \hat{q}_u = 1$) is estimated from the m -bin histogram of the target model, while $\hat{p}(y) = \{\hat{p}_u(y)\}_{u=1..m}$ (with $\sum_{u=1}^m \hat{p}_u = 1$) is estimated at a given location y from the m -bin histogram of the target candidate. Then at location y , the sample estimate of the Bhattacharyya coefficient for target density q and candidate density $p(y)$ is given by

$$\rho(y) \equiv \rho[\hat{p}(y), \hat{q}] = \sum_{u=1}^m \sqrt{\hat{p}_u \hat{q}_u}. \quad (12)$$

The distance between two distributions can be defined as

$$d(y) = \sqrt{1 - \rho[\hat{p}(y), \hat{q}]}. \quad (13)$$

3.2.2. Eye appearance model

To reliably characterize the intensity distribution of eyes and non-eyes, the intensity distribution is characterized by two images: even and odd field images, resulting from de-interlacing the original input images. They are under different illuminations, with one producing bright pupils and the other producing dark pupils as shown in Fig. 14. The use of two channel images to characterize eye



Fig. 14. The eye images: (A,B) left and right bright pupil eyes, (C,D) corresponding left and right dark pupil eyes.

appearance represents a new contribution and can therefore improve the accuracy of eye detection.

Thus, there are two different feature probability distributions of the eye target corresponding to dark pupil and bright pupil images respectively. We use a 2D joint histogram, which is derived from the grey level dark pupil and bright pupil image spaces with $m = l \times l$ bins, to represent the feature probability distribution of the eyes. Before calculating the histogram, we employ a convex and monotonic decreasing kernel profile k to assign a smaller weight to the locations that are farther from the center of the target. Let us denote by $\{x_i\}_{i=1 \dots n_h}$ the pixel locations of a target candidate that has n_h pixels, centered at y in the current frame. The probability distribution of the intensity vector $I = (I_b, I_d)$, where I_d and I_b represent the intensities in the dark and bright images, respectively, in the target candidate is given by

$$\hat{p}_u(y) = \frac{\sum_{i=1}^{n_h} k(\|\frac{y-x_i}{h}\|^2) \delta[b(x_i) - u]}{\sum_{i=1}^{n_h} k(\|\frac{y-x_i}{h}\|^2)} \quad \text{where } u = 1, 2, \dots, m \quad (14)$$

in which the $b(x_i)$ is the index to a bin in the joint histogram of the intensity vector I at location x_i , h is the radius of the kernel profile and δ is the Kronecker delta function. The eye model distribution q can be built in a similar fashion.

3.2.3. Algorithm

After locating the eyes in the previous frame, we construct an eye model \hat{q} using Eq. (14) based on the detected eyes in the previous frame. We then predict the locations y_0 of eyes at current frame using the Kalman filter. Then we treat y_0 as the initial position and use the mean shift iterations to find the most similar eye candidate to the eye target model in the current frame using the following algorithm:

1. Initialize the location of the target in the current frame with y_0 , then compute the distribution $\{\hat{p}_u(y_0)\}_{u=1 \dots m}$ using Eq. (14) and evaluate similarity measure (Bhattacharyya coefficient) between the model density \hat{q} and target candidate density \hat{p}

$$\rho[\hat{p}(y_0), \hat{q}] = \sum_{u=1}^m \sqrt{\hat{p}_u(y_0) \hat{q}_u}. \quad (15)$$

2. Derive the weights $\{w_i\}_{i=1 \dots n_h}$ according to

$$w_i = \sum_{u=1}^m \delta[b(x_i) - u] \sqrt{\frac{\hat{q}_u}{\hat{p}_u(y_0)}}. \quad (16)$$

3. Based on the mean shift vector, derive the new location of the eye target

$$y_1 = \frac{\sum_{i=1}^{n_h} x_i w_i g(\|\frac{y_0-x_i}{h}\|^2)}{\sum_{i=1}^{n_h} w_i g(\|\frac{y_0-x_i}{h}\|^2)}, \quad (17)$$

where $g(x) = -k'(x)$ and then update $\{\hat{p}_u(y_1)\}_{u=1 \dots m}$, and evaluate

$$\rho[\hat{p}(y_1), \hat{q}] = \sum_{u=1}^m \sqrt{\hat{p}_u(y_1) \hat{q}_u}. \quad (18)$$

4. While $\rho[\hat{p}(y_1), \hat{q}] < \rho[\hat{p}(y_0), \hat{q}]$. Do $y_1 \leftarrow 0.5(y_0 + y_1)$. This is necessary to avoid the mean shift tracker moving to an incorrect location.
5. If $\|y_1 - y_0\| < \varepsilon$, stop, where ε is the termination threshold. Otherwise, set $y_0 \leftarrow y_1$ and go to step 1.

The new eye locations in the current frame can be achieved in a few iterations compared to the correlation based approaches, which must perform an exhaustive search around the previous eye location. Due to the simplicity of the calculations, it is much faster than correlation. Fig. 15B plots the surface for the Bhattacharyya coefficient of the large rectangle marked in Fig. 15B. The mean shift algorithm exploits the gradient of the surface to climb, from its initial position, to the closest peak that represents the maximum value of the similarity measure.

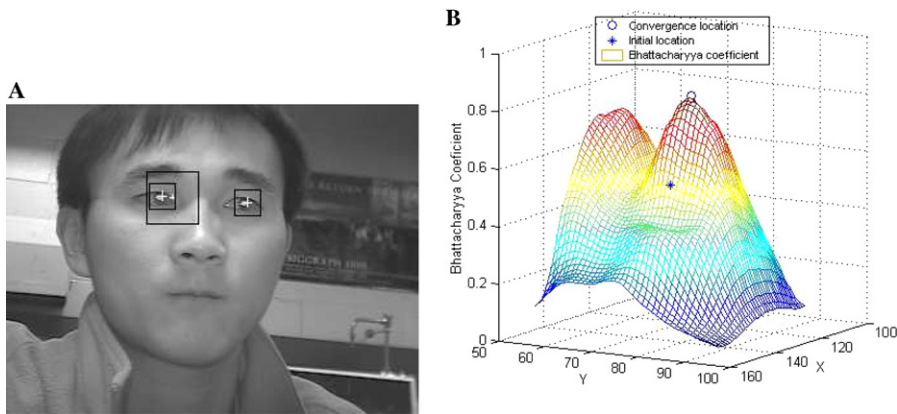


Fig. 15. (A) The image frame 13; (B) Values of Bhattacharyya coefficient corresponding to the marked region (40×40 pixels) around the left eye in frame 13. Mean shift algorithm converges from the initial location (*) to the convergence point (O), which is a mode of the Bhattacharyya surface.

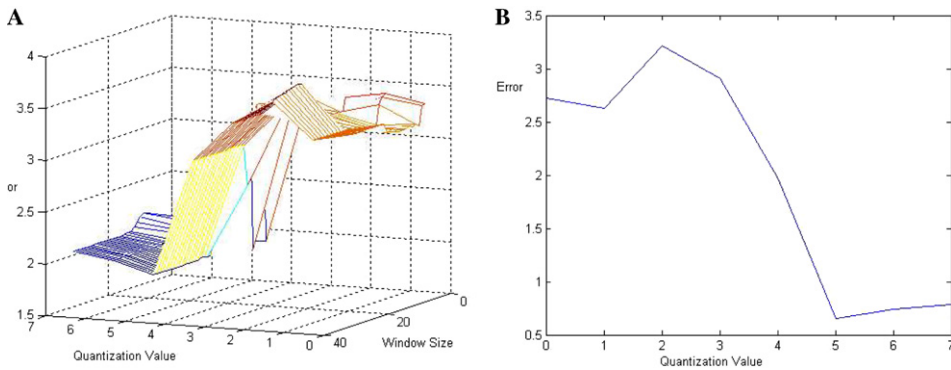


Fig. 16. The error distribution of tracking results: (A) error distribution vs. intensity quantization values and different window sizes; (B) error distribution vs. quantization levels only.

3.2.4. Mean shift tracking parameters

The mean shift algorithm is sensitive to the window size and the histogram quantization value. In order to obtain the best performance of the mean shift tracker for a specific task, we have to find the appropriate histogram quantization value and the proper window size. We choose several image sequences and manually locate the left eye positions in these frames. Then we run the mean shift eye tracker under different

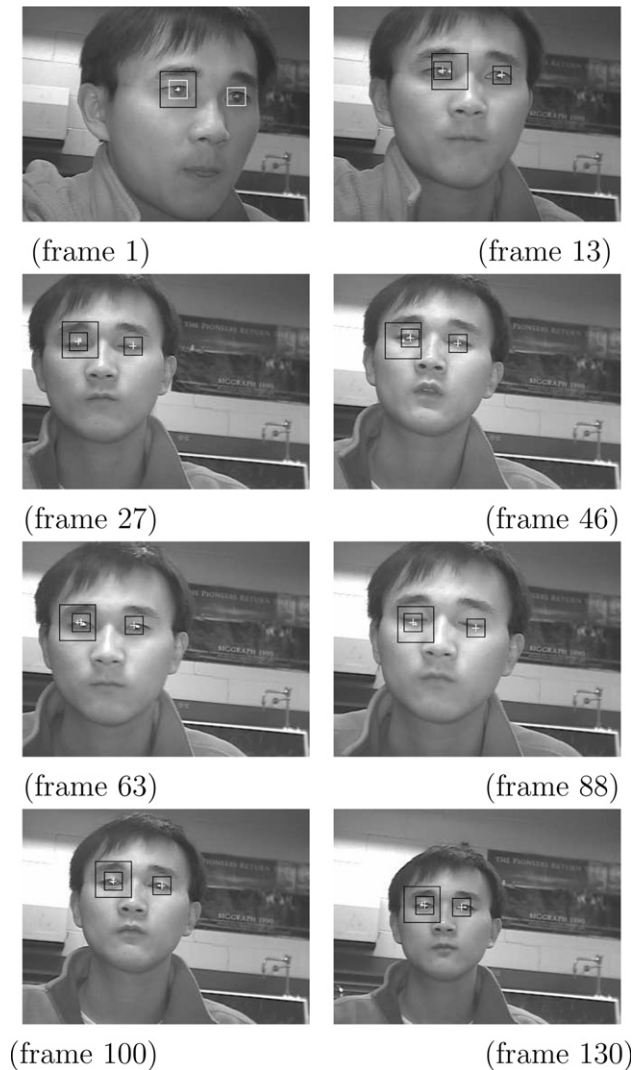


Fig. 17. Mean shift tracking both eyes with initial search area of 40×40 pixels, as represented by the large black rectangle. The eyes marked with white rectangles in frame 1 are used as the eye model and the tracked eyes in the following frames are marked by the smaller black rectangles.

window sizes and different histogram quantization values, we evaluate the performance of mean shift eye tracker under those conditions using the following criterion:

$$\alpha_{\text{error}} = \sum_{i=1}^N \sqrt{(y_i(\text{tracked}) - y'_i(\text{manual}))^2} / N, \quad (19)$$

where N is the number of image frames and $y_i(\text{tracked})$ is the left eye location tracked by mean shift tracker in the image frame i ; $y'_i(\text{manual})$ is the left eye location manually located by the person in the image frame i . We treat the manually selected eye locations as the correct left eye locations.

The intensity histogram is scaled in the range of $0-255/(2^q)$, q is the quantization value. The results are plotted in Fig. 16. From Figs. 16A and B, we can determine the optimal quantization level to be 2^5 while the optimal window size is 20×20 pixels. Fig. 17 shows some tracking results with these parameters.

The mean-shift tracker, however, is sensitive to its initial placement. It may not converge or converge to a local minimum if placed initially far from the optimal location. It usually converges to the mode, closest to its initial position. If the initial location is in the valley between two modes, the mean shift may not converge to any (local maxima) peaks as shown in Fig. 18. This demonstrates the sensitivity of mean-shift tracker to initial placement of the detector.

3.2.5. Experiments on the mean shift eye tracking

To study the performance of the mean-shift tracker, we apply it to sequences that contain images with weak or partially occluded or no bright pupils. We noticed when bright pupils disappear due to either eye closure or face rotations as shown in Fig. 19, the Kalman filter fails because there are no bright pupil blobs in the difference

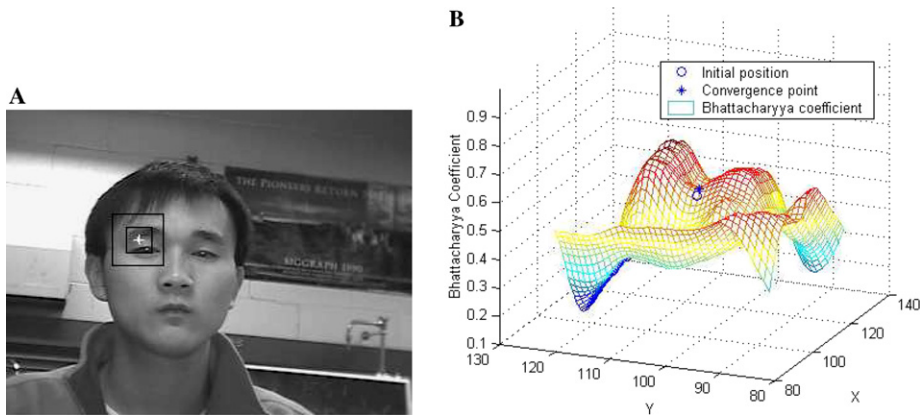


Fig. 18. (A) Image of frame 135, with the initial eye position marked and initial search area outlined by the large black rectangle. (B) Values of Bhattacharyya coefficient corresponding to the marked region (40×40 pixels) around the left eye in (A). Mean shift algorithm can not converge from the initial location (O) (which is in the valley of two modes) to the correct mode of the surface. Instead, it is trapped in the valley.

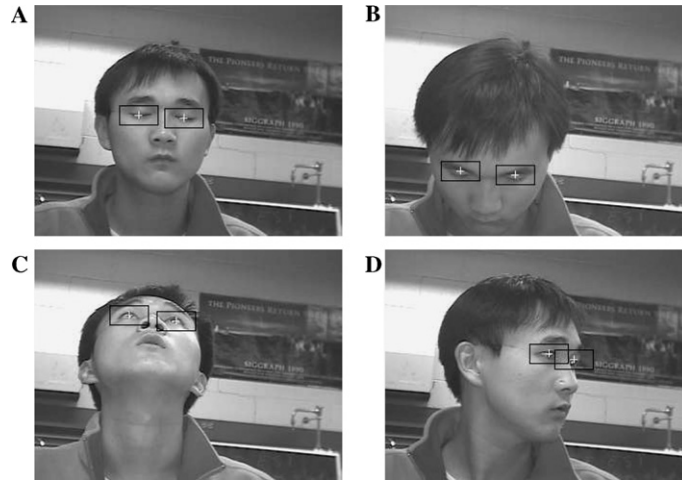


Fig. 19. Bright pupil based Kalman tracker fails to track eyes due to absence of bright pupils caused by either eye closure or oblique face orientations. The mean shift eye tracker, however, tracks eyes successfully as indicated by the black rectangles.

images. However the mean shift tracker compensates for the failure of bright pupil tracker because it is an appearance based tracker that tracks the eyes according to the intensity statistical distributions of the eye regions and does not need bright pupils. The black rectangles in Fig. 19 represent the eye locations tracked by the mean shift tracker.

4. Combining Kalman filtering tracking with mean shift tracking

The mean shift tracking is fast and handles noise well. But it is easily distracted by nearby similar targets such as the nearby region that appears similar to the eyes. This is partially because of the histogram representation of the eyes appearance, which does not contain any information about the relative spatial relationships among pixels. The distraction manifests primarily as errors in the calculated center of the eyes. The mean shift tracker does not have the capability of self-correction and the errors therefore tend to accumulate and propagate to subsequent frames as tracking progresses and eventually the tracker drifts away. Another factor that could lead to errors with eye tracking based on mean shift is that the mean shift tracker cannot continuously update its eye model despite the fact that the eyes look significantly different under different face orientations and lighting conditions as demonstrated in the left column of Fig. 20. We can see that the mean shift eye tracker cannot identify the correct eye location when the eyes appear significantly different from the model eyes images due to face orientation change.

To overcome these limitations with mean shift tracker, we propose to combine the Kalman filter tracking with the mean shift tracking to overcome their respective

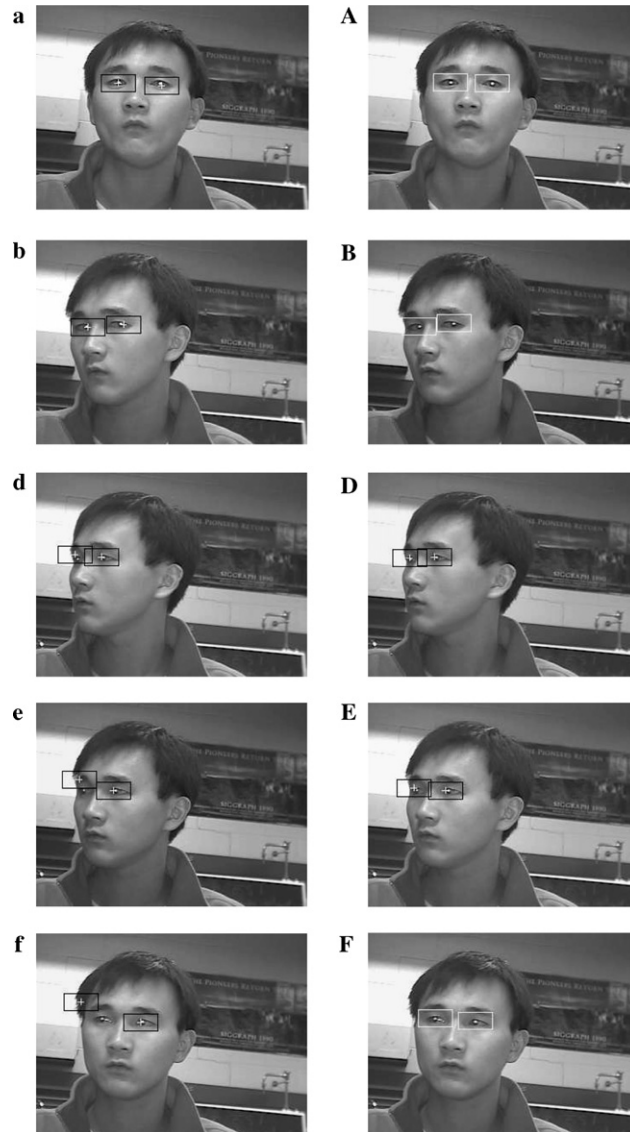


Fig. 20. An image sequence to demonstrate the drift-away problem of the mean shift tracker as well as the correction of the problem by the integrated eye tracker. Frames (a, b, d, e, and f) show the drift away case of the mean Shift eye tracker; for the same image sequences, (A, B, D, E, and F) shows the improved results of the combined eye tracker. White rectangles show the eyes tracked by the Kalman tracker while the black rectangles show the tracked eyes by the mean shift tracker.

limitations and to take advantage their strengths. The two trackers are activated alternately. The Kalman tracker is first initiated, assuming the presence of the bright pupils. When the bright pupils appear weak or disappear, the mean shift tracker is

activated to take over the tracking. Mean shift tracking continues until the reappearance of the bright pupils, when the Kalman tracker takes over. To avoid the mean shift tracker drift away, the target eye model is continuously updated by the eyes successfully detected by the Kalman tracker. The right column of Fig. 20 shows the results of tracking the same sequence with the integrated eye tracker as the one shown on left column. It is apparent that the integrated tracker can correct the drift problem of the mean shift tracker.

5. Experimental results

In this section, we will present results from an extensive experiment we conducted to validate the performance of our integrated eye tracker under different conditions.

5.1. Eye tracking under significant head pose changes

Here, we show some qualitative and quantitative results to demonstrate the performance our tracker under different face orientations. Fig. 21 visually shows the typical tracking results for a person undergoing significant face pose changes, where the black rectangles represent the mean-shift tracker while the white rectangles represent the Kalman filter tracker.

Additional results for different subjects under significant head rotations are shown in Fig. 22. We can see that under significant head pose changes, the eyes will be either partially occluded or the appearance of eyes will be significantly different from the eyes with frontal faces. But the two eye trackers alternate reliably, detecting the eyes under different head orientations, with eyes either open, closed or partially occluded.

To further confirm this quantitatively, we manually located the positions of the eyes for two typical sequences and they serve as the ground-truth eye positions. The tracked eye positions are then compared with the ground-truth data. The results are summarized in Tables 2 and 3. From the tracking statistics in Tables 2 and 3, we can conclude that the integrated eye tracker is much more accurate than the Kalman filter pupil tracker, especially for the closed eyes and partially occluded eyes due to face rotations. These results demonstrate that this combination of two tracking techniques produces much better tracking results than using either of them individually.

5.2. Eye tracking under different illuminations

In this experiment, we demonstrate the performance of our integrated tracker under different illumination conditions. We vary the light conditions during the tracking. The experiment included first turning off the ambient lights, followed by using a mobile light source and positioning it close to the people to produce strong external light interference. The external mobile light produces significant shadows as well as intensity saturation on the subject's faces. Fig. 23 visually shows the sample tracking results for two individuals. Despite these somewhat extreme conditions, our eye tracker managed to track the eyes correctly. Because of the use of IR, the faces

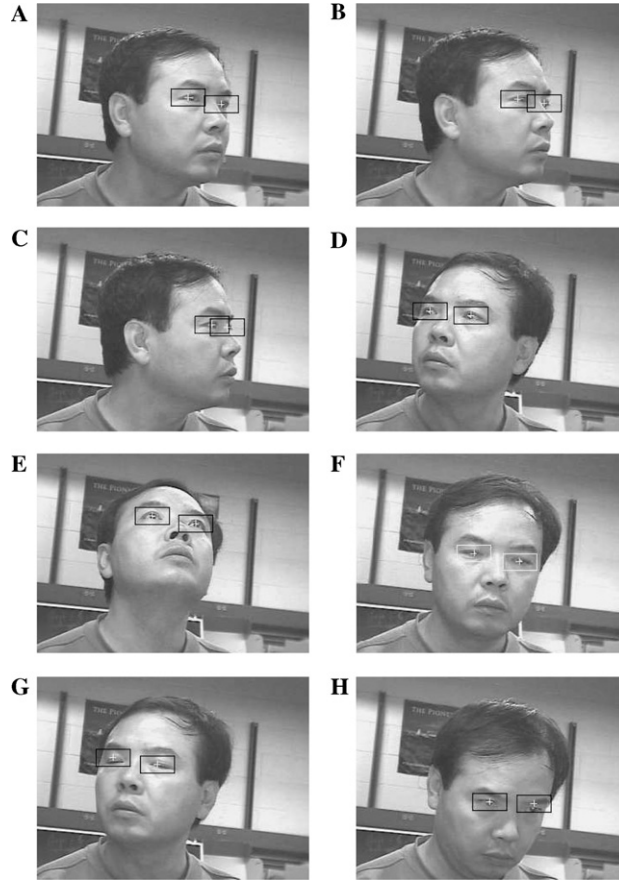


Fig. 21. Tracking results of the combined eye tracker for a person undergoing significant face pose change. White rectangles show the eyes tracked by the Kalman tracker while the black rectangles show the eyes tracked by the mean shift tracker.

are still visible and eyes are tracked even under darkness. It is apparent that illumination change does not adversely affect the performance of our technique as much. This may be attributed to the simultaneous use of active IR sensing, image intensity normalization for eye detection using SVM, and the dynamic eye model updating for the mean shift tracker.

5.3. Eye tracking with glasses

The significant eye appearance changes with glasses. Furthermore, the glares on the glasses caused by light reflections present significant challenges to eye tracking with glasses. In Fig. 24, we show the results of applying our eye tracker to persons wearing glasses. We can see that our eye tracker can still detect and track eyes



Fig. 22. Tracking results of the combined eye tracker for four image sequences (A), (B), (C), and (D) under significant head pose changes. White rectangles show the eyes tracked by the Kalman tracker while the black rectangles show the eyes tracked by the mean shift tracker.

Table 2

Tracking statistics comparison for both trackers under different eyes conditions (open, closed, and occluded) on the first person

Image 600 frames	Bright pupil tracker	Combined tracker
Left eye (open) 452 frames	400/452	452/452
Left eye (closed) 66 frames	0/66	66/66
Left eye (occluded) 82 frames	0/82	82/82
Right eye (open) 425 frames	389/425	425/425
Right eye (closed) 66 frames	0/66	66/66
Right eye (occluded) 109 frames	0/109	109/109

Table 3

Tracking statistics comparison for both trackers under different eyes conditions (open, closed, and occluded) on the second person

Image Sequence 1 600 frames	Bright pupil tracker	Combined tracker
Left eye (open) 421 frames	300/421	410/421
Left eye (closed) 78 frames	0/78	60/78
Left eye (occluded) 101 frames	0/101	60/101
Right eye (open) 463 frames	336/463	453/463
Right eye (closed) 78 frames	0/78	78/78
Right eye (occluded) 59 frames	0/59	59/59



Fig. 23. Tracking results of the combined eye tracker for two image sequences (A) and (B) under significant illumination changes. White rectangles show the eyes tracked by the Kalman tracker while the black rectangles show the eyes tracked by the mean shift tracker.



Fig. 24. Tracking results of the combined eye tracker for two image sequences (A,B) with persons wearing glasses. White rectangles show the eyes tracked by the Kalman tracker while the black rectangles show the eyes tracked by the mean shift tracker.

robustly and accurately for people with glasses. However, our study shows that when the head orientation is such that the glares completely occludes the pupils, our tracker will fail. This is a problem that we will tackle in the future.

5.4. Eye tracking with multiple people

Our eye tracker not only can track the eyes of one person but also can track multiple people's eyes simultaneously. Here, we show the results of applying our eye track-

er to simultaneously track multiple people's eyes with different distances and face poses to the camera. The result is presented in Fig. 25. This experiment demonstrates the versatility of our eye tracker.

5.5. Occlusion handling

Eyes are often partially or completely occluded either by face due to oblique face orientations or by hands or by other objects. A good eye tracker should be able to track eyes under partial occlusion and be able to detect complete occlusion and re-detect the eyes after the complete occlusion is removed. In Fig. 26, two persons are moving in front of the camera, and one person's eyes are occluded by another's head when they are crossing. As shown in Fig. 26, when the rear person moves from right to left, the head of the front person starts to occlude his eyes, beginning with one and then two eyes getting completely occluded. As shown, our tracker can still correctly track an eye even though it is partially occluded. When both eyes are completely occluded, our tracker detects this situation. As soon as the eyes reappear in the image, our eye tracker will capture the eyes one by one immediately as shown in Fig. 26. This experiment shows the robustness of our method to occlusions.

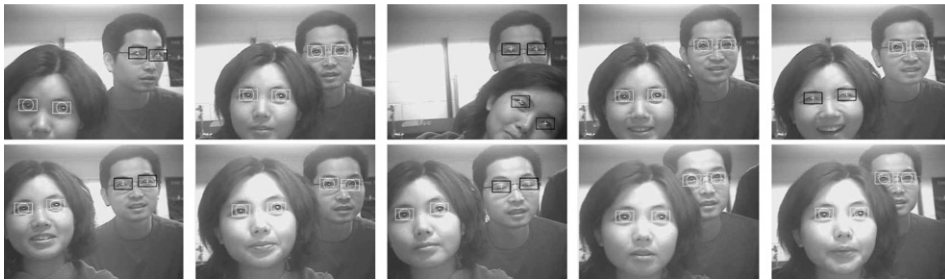


Fig. 25. Tracking results of the combined mean eye tracker for multiple persons. White rectangles show the eyes tracked by the Kalman tracker while the black rectangles show the eyes tracked by the mean shift tracker.

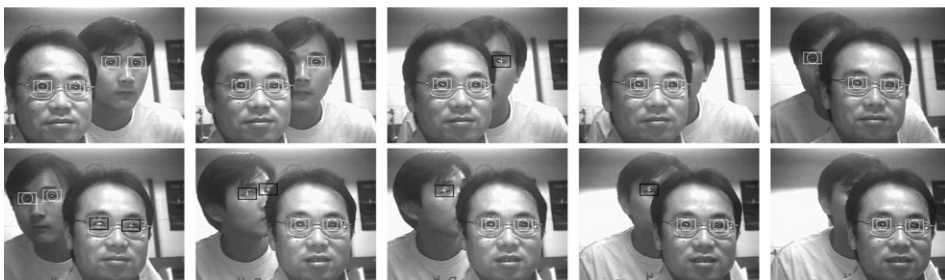


Fig. 26. Tracking results of combined eye tracker for an image sequence involving multiple persons occluding each other's eyes. White rectangles show the eyes tracked by the Kalman tracker while the black rectangles show the eyes tracked by the mean shift tracker.

6. Summary

In this paper, we present an integrated eye tracker to track eyes robustly under various illuminations and face orientations. Our method performs well regardless of whether the pupils are directly visible or not. This has been achieved by combining an appearance based pattern recognition method (SVM) and object tracking (Mean Shift) with a bright-pupil eye tracker based on Kalman filtering. Specifically, we take the following measures. First, the use of SVM for pupil detection complements with eyes detection based on bright pupils from IR illumination, allowing to detect eyes in the presence of other bright objects; second, two channels (dark-pupil and bright-pupil eye images) are used to characterize the statistical distributions of the eye, based on which a Mean Shift eye tracker is developed. Third, the eye model is continuously updated by the eye successfully detected from the last Kalman tracker to avoid error propagation with the mean shift tracker. Finally, the experimental determination of the optimal window size and quantization level for mean shift tracking further enhances the performance of our technique. Experiments show these enhancements have led to a significant improvement in eye tracking robustness and accuracy over existing eye trackers, especially under various conditions identified in Section 1. Furthermore, our integrated eye tracker is demonstrated to be able to handle occlusion, people with glasses, and to simultaneously track multiple people of different poses and scales.

The lessons we learn from this research are: (1) perform active vision (e.g., active IR illumination) to produce quality input images and to simplify the subsequent image processing; (2) combine different complementary techniques to utilize their respective strengths and to overcome their limitations, leading to a much more robust technique than using each technique individually.

Acknowledgments

This work is partially supported by a grant from AFOSR and a grant from Honda R&D Americas Inc., Mountain View, CA.

References

- [1] Q. Ji, X. Yang, Real time visual cues extraction for monitoring driver vigilance, in: *Proc. Int. Workshop on Computer Vision Systems*, Vancouver, Canada, 2001.
- [2] Q. Ji, Z. Zhu, Eye and gaze tracking for interactive graphic display, in: *Second Int. Symp. on Smart Graphics*, Hawthorne, NY, USA, 2002.
- [3] A. Yuille, P. Hallinan, D. Cohen, Feature extraction from faces using deformable templates, *Int. J. Comput. Vis.* 8 (2) (1992) 99–111.
- [4] X. Xie, R. Sudhakar, H. Zhuang, On improving eye feature extraction using deformable templates, *Pattern Recognit.* 27 (1994) 791–799.
- [5] K.M. Lam, H. Yan, Locating and extracting the eye in human face images, *Pattern Recognit.* 29 (1996) 771–779.
- [6] L. Zhang, Estimation of eye and mouth corner point positions in a knowledge-based coding system, in: *Proc. SPIE*, vol. 2952. Berlin, Germany, 1996, pp. 21–18.

- [7] M. Kampmann, L. Zhang, Estimation of eye, eyebrow and nose features in videophone sequences, in: *Int. Workshop on Very Low Bitrate Video Coding (VLBV 98)*, Urbana, USA, 1998.
- [8] G.C. Feng, P.C. Yuen, Variance projection function and its application to eye detection for human face recognition, *Int. J. Comput. Vis.* 19 (1998) 899–906.
- [9] G.C. Feng, P.C. Yuen, Multi-cues eye detection on gray intensity image, *Pattern Recognit.* 34 (2001) 1033–1046.
- [10] M. Nixon, Eye spacing measurement for facial recognition, in: *Proc. of the Society of Photo-Optical Instrument Engineers*, 1985.
- [11] P.W. Hallinan, Recognizing human eyes, in: *SPIE Proceedings*, vol. 1570, *Geometric Methods in Computer Vision*, 1991, pp. 212–226.
- [12] A. Pentland, B. Moghaddam, T. Starner, View-based and modular eigenspaces for face recognition, in: *Proc. IEEE Conf. on Computer Vision and Pattern Recognition (CVPR'94)*, Seattle, WA, 1994.
- [13] W. min Huang and R. Mariani, Face detection and precise eyes location, in: *Proc. Int. Conf. on Pattern Recognition (ICPR'00)*, 2000.
- [14] J. Huang, H. Wechsler, Eye detection using optimal wavelet packets and radial basis functions (rbfs), *Int. J. Pattern Recognit. Artif. Intell.* 13 (7) (1999) 1009–1025.
- [15] S. Kawato, J. Ohya, Two-step approach for real-time eye tracking with a new filtering technique, in: *Proc. Int. Conf. on System, Man & Cybernetics*, 2000, pp. 1366–1371.
- [16] S. Kawato, J. Ohya, Real-time detection of nodding and head-shaking by directly detecting and tracking the between-eyes, in: *Proc. 4th IEEE Int. Conf. on Automatic Face and Gesture Recognition*, 2000, pp. 40–45.
- [17] S. Kawato, N. Tetsutani, Real-time detection of between-the-eyes with a circle frequency filter, in: *Proc. of ACCV2002*, vol. I, 2002, pp. 442–447.
- [18] S. Kawato, N. Tetsutani, Detection and tracking of eyes for gaze-camera control, in: *Proc. 15th Int. Conf. on Vision Interface*, 2002.
- [19] Y. Tian, T. Kanade, J.F. Cohn, Dual-state parametric eye tracking, in: *Proc. 4th IEEE Int. Conf. on Automatic Face and Gesture Recognition*, 2000.
- [20] J. Waite, J. Vincent, A probabilistic framework for neural network facial feature location, *Br. Telecom Technol. J.* 10 (3) (1992) 20–29.
- [21] M. Reinders, R. Koch, and J. Gerbrands, Locating facial features in image sequences using neural networks, in: *Proc. Second Int. Conf. on Automatic Face and Gesture Recognition*, Killington, USA, 1997.
- [22] S.A. Sirohey, A. Rosenfeld, Eye detection, in: *Technical Report CAR-TR-896*, Center for Automation Research, University of Maryland, College Park, MD, 1998.
- [23] S.A. Sirohey, A. Rosenfeld, Eye detection in a face image using linear and nonlinear filters, *Pattern Recognit.* 34 (2001) 1367–1391.
- [24] B.D. Lucas, T. Kanade, An iterative image registration technique with an application to stereo vision, in: *International Joint Conference on Artificial Intelligence*.
- [25] M. Motwani and Q. Ji, 3d face pose discrimination using wavelets, in: *In Proceedings of IEEE International Conference on Image Processing*, Thessaloniki, Greece, 2001.
- [26] H. Schneiderman and T. Kanade, A statistical method for 3d object detection applied to faces and cars, in: *In IEEE Conference of Computer Vision and Pattern Recognition*, 2000.
- [27] Y. Ebisawa and S. Satoh, Effectiveness of pupil area detection technique using two light sources and image difference method, in: *Proceedings of the 15th Annual Int. Conf. of the IEEE Eng. in Medicine and Biology Society*, San Diego, CA, 1993, pp. 1268–1269.
- [28] Y. Ebisawa, Improved video-based eye-gaze detection method, *IEEE Trans. Instrument. Meas.* 47 (2) (1998) 948–955.
- [29] C. Morimoto, D. Koons, A. Amir, M. Flickner, Pupil detection and tracking using multiple light sources, *Technical Report RJ-10117*, IBM Almaden Research Center, 1998.
- [30] C. Morimoto, M. Flickner, Real-time multiple face detection using active illumination, in: *Proc. fourth IEEE Int. Conf. on Automatic Face and Gesture Recognition 2000*, Grenoble, France, 2000.

- [31] A. Haro, M. Flickner, I. Essa. Detecting and tracking eyes by using their physiological properties, dynamics, and appearance, in: *Proceedings IEEE CVPR 2000*, Hilton Head Island, South Carolina, 2000.
- [32] Lc Technologies. Available from: <<http://www.eyegaze.com>>.
- [33] Anon, Applied science laboratories. Available from: <<http://www.a-s-l.com.com>>.
- [34] Z. Zhu, Q. Ji, K. Fujimura, K. chih Lee, Combining Kalman filtering and mean shift for real time eye tracking under active ir illumination, in: *Int. Conf. on Pattern Recognition*, Quebec, Canada, 2002.
- [35] Z. Zhu, K. Fujimura, Q. Ji, Real-time eye detection and tracking under various light conditions, in: *Symposium on Eye Tracking Research and Applications*, New Orleans, LA, USA, 2002.
- [36] C. Cortes, V. Vapnik, Support-vector networks, *Mach. Learn.* 20 (1995) 273–297.
- [37] J. Huang, D. Ii, X. Shao, H. Wechsler, Pose discrimination and eye detection using support vector machines (svms), in: *Proc. of NATO-ASI on Face Recognition: From Theory to Applications*, 1998, pp. 528–536.
- [38] D. Comaniciu, V. Ramesh, P. Meer, Real-time tracking of non-rigid objects using mean shift, in: *IEEE Conf. on Comp. Vis. and Pat. Rec.*, Hilton Head Island, South Carolina, 2000.
- [39] T.E. Hutchinson, Eye movement detection with improved calibration and speed. U.S. patent 4950069.
- [40] Q. Ji, X. Yang, Real-time eye, gaze, and face pose tracking for monitoring driver vigilance, in: *Real-Time Imaging*, 2002, pp 357–377.
- [41] A.W. Fitzgibbon, R.B. Fisher, A buyers guide to conic fitting, in: *Proc. fifth British Machine Vision Conference*, 1995, pp. 513–522.
- [42] A. Blake, R. Curwen, A. Zisserman, A framework for spatio-temporal control in the tracking of visual contours, *Int. J. Comput. Vis.* 11 (2) (1993) 127–145.
- [43] P.S. Maybeck *Stochastic Models, Estimation and Control*, vol. 1, Academic Press, 1979.